Investigation of Waves Generated by Tropical Cyclone Kyarr in the Arabian Sea: An Application of ERA5 Reanalysis Wind Data

Aliasghar Golshani [1],*, Masoud Banan-Dallalian [2], Mehrdad Shokatian-Beiragh [2], Majid Samiee-Zenoozian [2] and Shahab Sadeghi-Esfahlani [2]

[1] Faculty of Civil and Earth Resources Engineering, Islamic Azad University, Central Tehran Branch, Tehran 1131833116, Iran
[2] Department of Water Resources Engineering, Faculty of Civil Engineering, University of Tabriz, Tabriz 5166616471, Iran
* Correspondence: ali.golshani@iauctb.ac.ir

Abstract: In this study, the wave conditions in the Arabian Sea induced by tropical cyclone Kyarr (2019) have been simulated by employing the 3rd generation wave model MIKE 21 SW. The model was run from 24 October to 1 November 2019, a total of 8 days. The MIKE 21 SW model was forced by reanalyzed ERA5 wind data from the European Centre for Medium-Range Weather Forecasts (ECMWF). The results are compared with buoy data from the Indian National Centre for Ocean Information Services (INCOIS), which is located at 67.44° E, 18.50° N. In addition, the satellite altimeter data (CryoSat-2, SARAL and Jason-3 satellite altimeter data) was utilized for validation. Three wave parameters are considered for the validation: the significant wave height; the peak wave period; and the mean wave direction. The validation results showed that the significant wave height, the peak wave period, and the mean wave direction could be reasonably predicted by the model with reanalysis wind data as input. The maximum significant wave height reached to 10.7 m (with an associated peak wave period of 12.5 s) on 28 October 2019 at 23:00:00 in the middle of the Arabian Sea. For coastal areas, the significant wave height along the Iran and Pakistan (north Arabian Sea) coasts increased to a range of 1.4–2.8 m when tropical cyclone Kyarr moved northward. This wave height along with elevated sea level may cause severe coastal erosion and nearshore inland flooding. Impacts of cyclones on coastal zones critical facilities and infrastructure can be reduced by timely and suitable action before the event, so coastal managers should understand the effect of cyclones and their destructive consequences. The validated model developed in this study may be utilized as input data of evaluating the risk to life and infrastructure in this area.

Keywords: tropical cyclone Kyarr; ERA5; reanalysis wind data; wave model

1. Introduction

Tropical cyclones affect a large portion of the world's coasts and are often linked with catastrophic consequences for coastal populations and extensive infrastructural damage [1–3]. Tropical cyclones form over warm, humid ocean waters close to the equator because they are linked with warm, humid air. The rising warm and humid air creates a zone of lower pressure underneath. Cooler air rises when it enters the lower pressure region and becomes humid. When warm, humid air ascends, it cools and condenses into clouds. The entire system of winds and clouds swirls and develops due to the heat and evaporation of the seas. Cyclones need at least 26.5 °C ocean water temperatures to form and expand through a relatively deep layer (approximately 50 m) [4]. Cyclones that form above the equator rotate counterclockwise, while those that originate below the equator rotate clockwise, due mainly to the Earth's axis of rotation. As a result, cyclones are linked with a significant pressure gradient, generating powerful winds, and storm surges. The extent of a tropical cyclone's damage is determined by its strength, size, and position [5].

Cyclones can cause a high death toll and severe damage to property, ecosystems and maritime infrastructure [6]. Numerous municipalities situated along the shore, have a sizeable population with accompanying commercial areas and industrial centers, making them very important [7,8]. Cyclones create a significant hazard to human life and property in coastal regions, particularly densely populated low-lying regions.

In the Arabian Sea, approximately 29 significant tropical cyclones have occurred since 1945. In 1977, a cyclone hit the Masirah Island and south Omani coasts killing almost one hundred people and demolishing many dwellings [9]. In 2002, a tropical cyclone affected the south of the Arabian Peninsula, resulting in the region's highest rainfall in 30 years [10]. In 2007, the Gonu tropical cyclone (the most significant storm to ever form in the Arabian Sea) killed 23 people off the south coast of Iran and 49 people off the coast of Oman. Additionally, the storm caused $4 billion in economic damage to Oman and approximately $215 million in damage to Iran [11]. Cyclones Phet in 2010, Nilofar in 2015, Mekunu in 2018, and Kyarr in 2019 were other powerful tropical cyclones that affected the Arabian Sea and surrounding countries. Therefore, it is crucial to assess the effects of cyclones and to simulate them to identify the most dangerous zones along the coastlines for future planning and management.

Tropical cyclones that form in the Arabian Sea, regularly affect the northern Indian Ocean throughout the summer, although they seldom enter the north Arabian Sea or Gulf of Oman [12–14]. On 30 October 2019, Kyarr cyclone originated approximately 1400 km east of the Sultanate of Oman (Figure 1). It moved north-westward and developed into a Category 4 cyclone (Based on Saffir–Simpson scale) on 26 October. On 27 October, it achieved the maximum wind speed of 131 km/h and the minimum central pressure of 923 mbar. On 30 October, it began propagating southwest, gradually losing its strength until it faded into a tropical depression on 31 October [15]. Although this tropical cyclone did not move to the Gulf of Oman, extreme erosion of shorelines and flooding of roadways, coastal developments, and other coastal infrastructures across the east coast of the United Arab Emirates were observed due to the unfavorable co-occurrence of cyclonic waves and spring tides.

Dibajnia et al. [16] assessed the maximum wave heights of the Arabian Sea during the Gonu cyclone. Sarker [17], conducted an investigation on determining the maximum wave height caused by the Nilofar cyclone in the Arabian Sea by using MIKE 21 model. The model performance was evaluated at a measurement point at Chabahar Bay in Iran at 30 m depth. Bakhtiari et al. [18] used the 2D MIKE 21 model to evaluate recent storms in the Arabian Sea, including the Gonu cyclone and evaluated the results of the wave and hydrodynamic models using observed data in the Oman Gulf. As well, computer simulations and field observations have been used to predict the wave characteristics associated with cyclones [19–26]. Global reanalyzed wave and wind data is widely used in ocean and marine hindcasting [27–29]. Hodges et al. [30] demonstrated that global models lack the precision required to accurately replicate the atmospheric fields of low frequency high impact extreme conditions, such as tropical cyclones, a weakness that is also transmitted to upper-tail storm surge levels, which are typically overestimated by reanalyses. Pan et al. [31] developed methods and utilized reanalyzed data to enhance tropical cyclones wind field forecast. In comparison to the global wind model and reanalysis data, the results demonstrated an improvement in the hindcasting of wind fields. However, the European Centre for Medium-Range Weather Forecasts (ECMWF) ERA5 is one of the most reliable and comprehensive of the global-gridded reanalysis meteorological datasets [32].

Reanalysed data is widely believed to underestimate the wind field during cyclones and as a result is not generally suggested as the primary input data for cyclone simulation [22]. However, for studies with the aim of simulating the waves at a location far from the storm center, it was helpful in investigating the use of hindcast data as wave model in this study. ECMWF ERA5 is the 5th generation ECMWF atmospheric reanalysis of global climate since January 1950. ERA5 provides hourly estimates of a variety of atmospheric, land, and oceanic climate variables. This paper employs ECMWF ERA5 reanalysis wind

data to investigate the wave model during Cyclone Kyarr in the Arabian Sea. The aim of this study is to describe wave pattern induced by Cyclone Kyarr using MIKE 21 SW numerical model and to examine the suitability of the ECMWF ERA 5 data for wave modeling under hurricane conditions. Considering the increase of the resolution of ECMWF wind data products in recent years, the novelty of this study is to investigate the effectiveness of ECMWF ERA5 wind data with resolution of 0.25 for wave modeling.
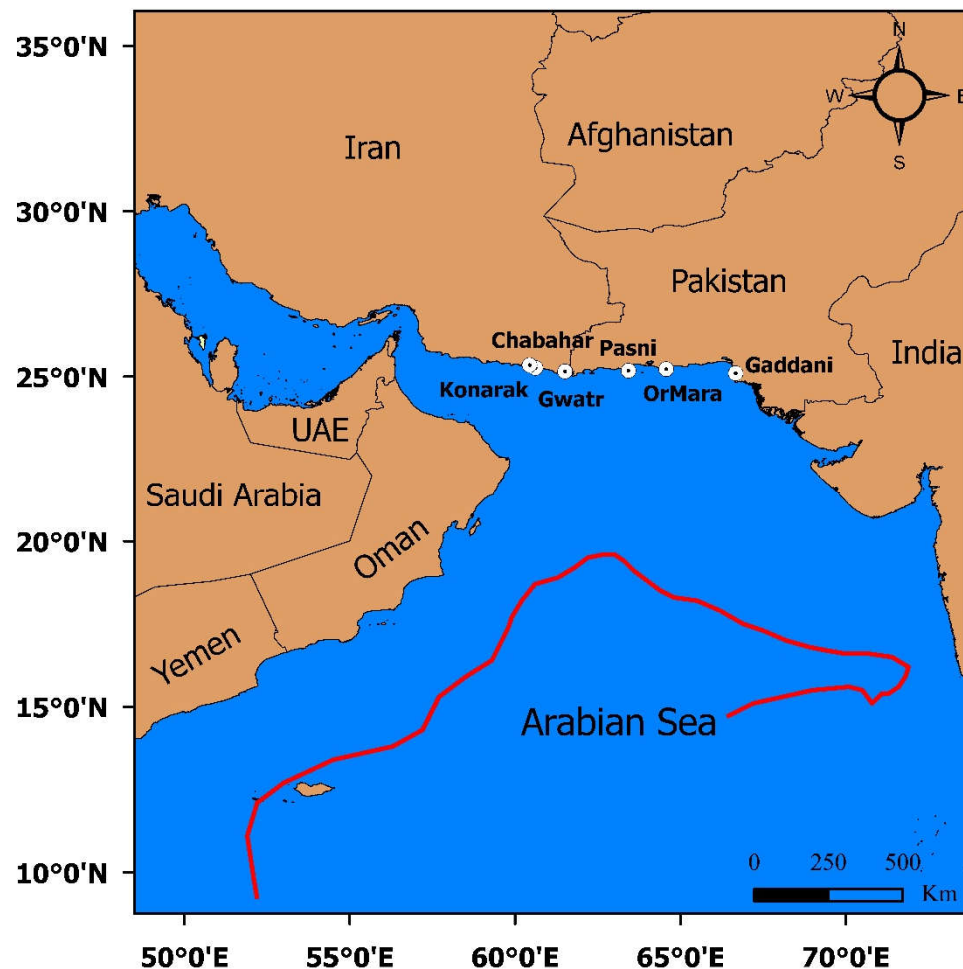

Figure 1. Tropical cyclone Kyarr track in the Arabian Sea (2019).

2. Materials and Methods

2.1. Study Area/Meteorological Conditions

The Arabian Sea is an area of the northern Indian Ocean that is constrained on the north by Iran, the Gulf of Oman and Pakistan; on the west by the Gulf of Aden, the Arabian Peninsula, and the Guardafui Channel; on the southwest by the Somali Sea; on the southeast by the Laccadive Sea; and on the east by India. It covers an area of 3,862,000 km^2 and reaches a maximum depth of 4652 m.

Summer and winter monsoons strongly affect the circulation pattern throughout the Arabian Sea. The winter monsoon lasts from November to April characterized by northeasterly winds averaging 5 m/s, while the summer monsoon lasts from July to September characterized by southerly and southwesterly winds with an average speed of 15 m/s. The remaining months are called post-monsoon (October) or pre-monsoon (May and June) [33]. Most of the tropical cyclones in the Arabian Sea form during in pre-monsoon (May) and post-monsoon (October and November) seasons. Nevertheless, some cyclones form between June and early September [34]. The monthly averages of daily average wind speeds during the Kharif season (March to June) in the Gulf of Oman were derived from

reanalysis data (1981 to 2019) by the ECMWF. During the Kharif season, wind grew in strength and reached up to 4 m/s, with the North Northeast (NNE) being the predominant wind direction (Figure 2).
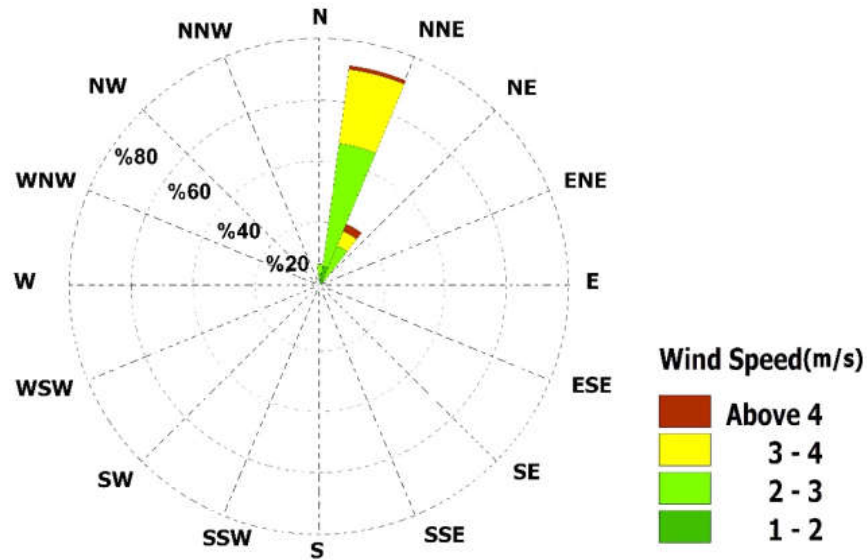

Figure 2. Wind rose for the Gulf of Oman in Kharif season (1981–2019).

    Figure 3 illustrates the frequency of very severe cyclonic storms in the north Indian Ocean, which encompasses the Bay of Bengal and the Arabian Sea, over the last 120 years based on IMD categorizing, which can be found in http://imd.gov (accessed on 27 May 2017) in [35]. According to the data analysis, 298 severe cyclonic storms have been recorded for the north Indian Ocean up to the present. October and November recorded total severe cyclonic storms of 53 and 85, respectively, whereas May and June reported overall of 60 and 20, respectively (CWRC, 2011). Additionally, the annual probability of intensification from depression to cyclonic storm was 44.8% during the last 125 years, 21.2% from depression to severe cyclonic storms, and 47.3% from cyclonic storm to severe cyclonic storms. March–April–May had the most probable of intensification (71.4%, 78%, and 69.9%, respectively) for depressions that ultimately changed to cyclonic storms, whereas October–November–December had the lowest probability of intensification (50%, 67.6%, and 59.8% respectively).
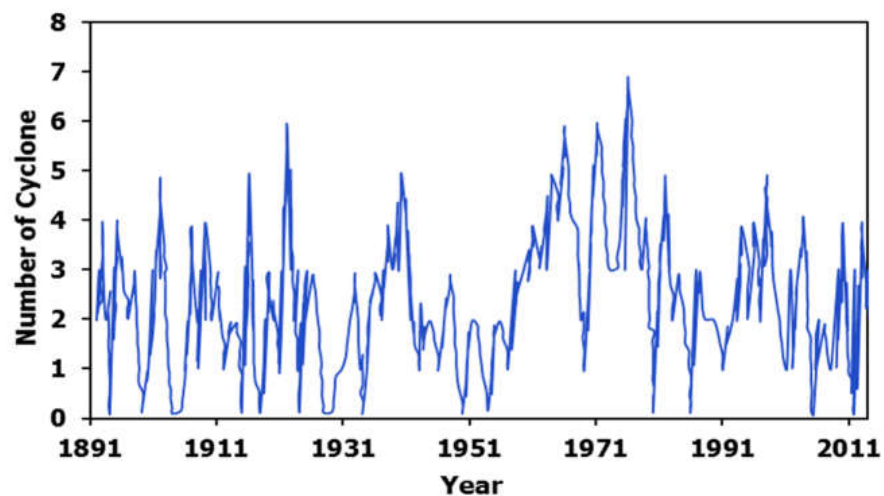

Figure 3. Frequency of very severe cyclones (1891–2011).

Apart from the Kyarr, four additional Category 4 or greater tropical storms have been reported in the Arabian Sea since 1998, as per the NOAA's Historical Hurricane Tracks Database: Phet, 2010 (145 mph winds), Nilofar, 2014 (130 mph winds), Chapala, 2015 (140 mph winds), and Gonu, 2007 (165 mph winds, the Arabian Sea's only Category 5 recorded). In this study, the numerical model was forced by reanalysis ERA5 wind data from the ECMWF. The Figure 4 illustrates the wind field generated by the ECMWF data as it passed over the Arabian Sea at four different locations of cyclone eye (Table 1).
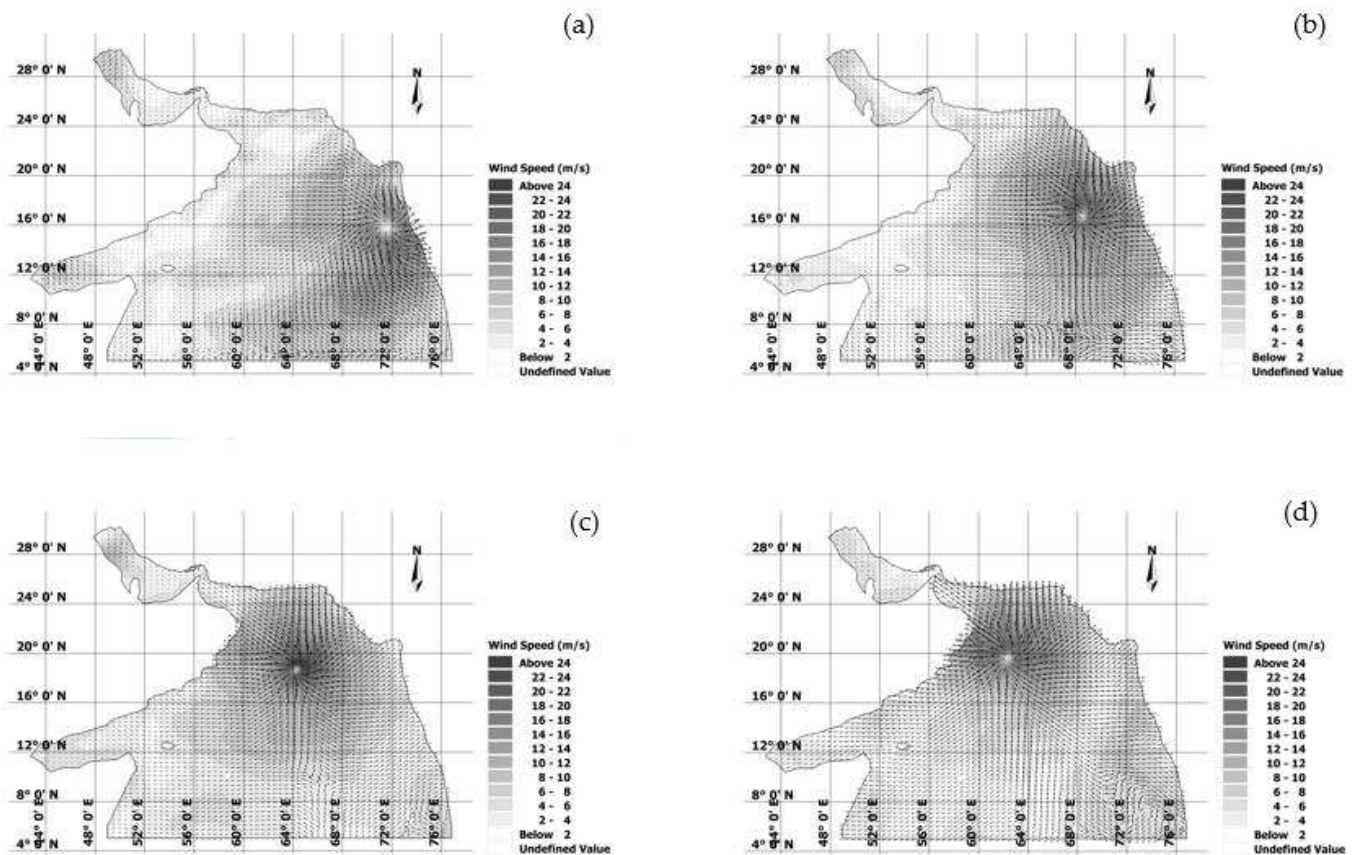

Figure 4. Tropical cyclone Kyarr wind field (based on ECMWF data) over the Arabian Sea at different times mentioned in Table 1; a darker gray color indicates a higher wind speed. (X and Y axis show the longitude and latitude, respectively). (**a**) 24 October, (**b**) 26 October, (**c**) 27 October and (**d**) 29 October.

Table 1. Track statistics related to four timesteps of tropical cyclone Kyarr illustrated in Figure 4.

	Date	Time	Lat.	Lon.	Wind Speed (m/s)	Category
Formation (a)	24 October	18:30 GMT	15.8	71.3	17.88	-
Reclassified as a Category 4 cyclone (b)	26 October	18:30 GMT	16.8	68.9	58	4
Highest wind speed (1 min sustained) (c)	27 October	12:00 GMT	17.5	66.8	69	4
Reclassified as a Category 3 cyclone (d)	29 October	12:00 GMT	19.5	63	53	3

2.2. General Aspects (Numerical Model)

The MIKE 21 Spectral Wave Model (Mike 21 SW) is a 3rd generation spectral wind-wave model based on unstructured mesh developed by the Danish Hydraulic Institute. The model simulates the growth, decay and transformation of wind-generated waves and

swells in coastal regions. The model contains the following components: wave growth caused by wind, nonlinear wave-wave interaction, dissipation caused by white-capping, dissipation caused by bottom friction, dissipation caused by wave breaking, shoaling and refraction caused by depth variations, wave-current interaction and the effect of changing water depths over the time, as well as drying and flooding. The model employs the wave action balance equation which uses the spectrum of wave action density to describe the wave field. The model is based on numerical integration of the equation for the balance of wave action in Cartesian coordinates [36,37].

This study provides an estimation of the wave characteristics of the Arabian Sea during the 2019 tropical cyclone Kyarr. The bathymetry and computational domain are shown in Figure 5. The considered region covers the latitudes of 5 to 30 N and longitudes of 43 to 76.5 E, with a resolution of 100 km for large elements but the element resolution becomes finer towards the cyclone track with the smallest resolutions of approximately 1 km. Additionally, a total of 236,677 nodes considered to encompass the study area adequately. Bathymetry data for the area is provided by merging data from two sources. Firstly, the 1 arc-minute global relief model of Earth's surface that integrates land topography and ocean bathymetry (Etopo1) and secondly, the MIKE C-MAP with the scale of 1:50,000.
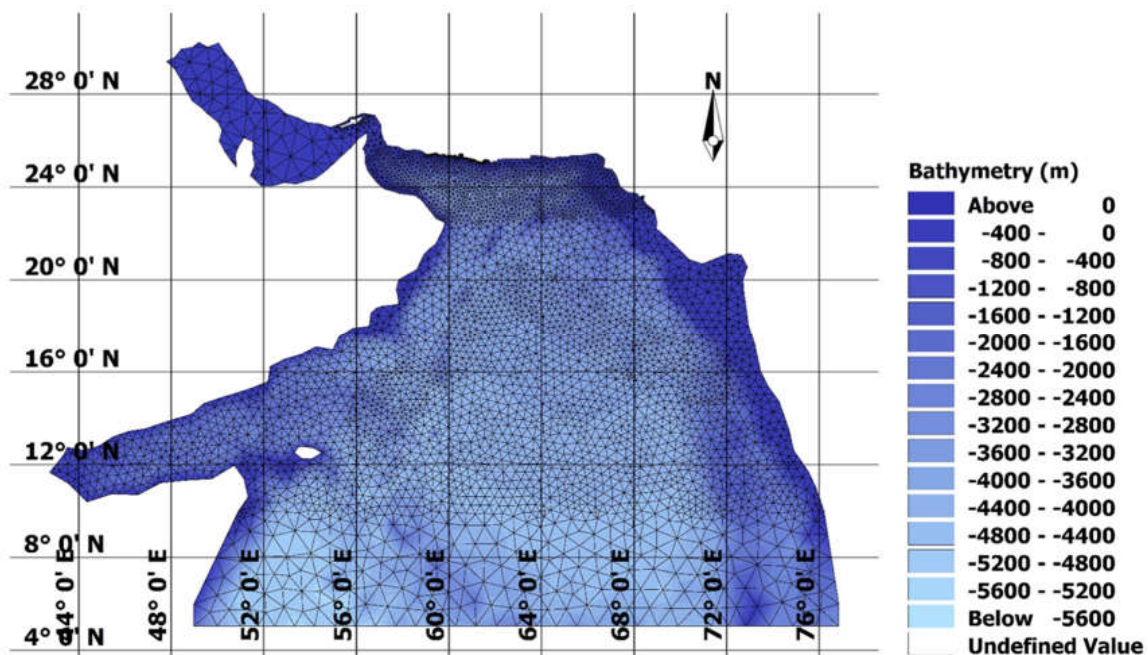

Figure 5. Computational domain and bathymetry.

2.2.1. The Governing Equation of MIKE21 SW

By solving the energy transfer equation along with the source and sink terms, the MIKE 21 SW is derived. The wave model's governing equation is defined in terms of the wave action density spectrum $N(\sigma,\theta)$ (Equation (1)).

$$N(\sigma.\theta) = \frac{E}{\sigma},$$ (1)

where θ denotes the wave propagation direction, and σ is the independent phase parameter. E represents the energy density [38].

In the wave model of this study, S (energy source) represents an interaction between multiple source functions that describe various physical phenomena (Equation (2)).

$$S = Sin + Swc + Snl + Sbf + Sbr,$$ (2)

where S_{wc} and S_{br} are the dissipation of wave energy caused by the white-capping and depth-induced breaking, meanwhile S_{in} is the wind generated energy and S_{nl} represents the energy transfer by nonlinear wave–wave interactions.

2.2.2. Input Wind Data

A precise wind field is critical for wave modeling since it is the wind that produces shear stresses, which in turn make waves, currents and surges. Analytical formulas are often used to estimate the 2D pressure and wind fields inside a tropical cyclone (Vortex model). Numerous studies have implemented such models to create input circumstances and correctly predict storm surge occurrences caused by cyclones [39–43]. On the other hand, analytical vortex models assume an idealistic cyclone and ignore interactions with other meteorological systems, which results in an incorrect depiction of the wind field distant from the cyclone center [44]. To fill these gaps, wind and pressure input data was collected with a temporal resolution of one hour and a spatial resolution of 0.25° from the ECMWF ERA5 dataset from 24 October to 1 November 2019 in the study area. It should be noted that global wind models have specific resolutions, so they are not accurate in the cyclone's path. The use of global wind models will produce inaccurate results if the cyclone passes close to the study area (the resolution of the wind model must be small enough to achieve accurate results, while as mentioned, the global wind models have a fixed resolution in the whole world). As shown in Figure 1, the path of tropical cyclone Kyarr was far from the coasts of Makran, so the global model can be employed with confidence.

2.2.3. Boundary Condition

The significant wave height, the peak wave period and the mean wave direction were the boundary conditions which were extracted from the ECMWF ERA5 dataset with a temporal resolution of one hour and a spatial resolution of 0.5°. The wave parameters were imported to the wave model's open boundary (5° N).

2.3. Model Calibration and Validation

The MIKE 21 SW model was run for eight days, from 24 October through 1 November, 2019. In this study, the modeled wave characteristics were compared to the buoy wave data (Indian National Centre for Ocean Information Services (INCOIS)). Three-hourly buoy wave data at AD06 station, which is situated at approximately 67.44° E, 18.50° N was used for the duration of tropical cyclone Kyarr. The MIKE 21 model was calibrated by minimizing the wave height simulation error. The calibration parameter was the whitecapping dissipation rate. In deep seas, the whitecapping dissipation rate is often employed as the parameter of calibration in deep waters [45–47]. Furthermore, the study of model sensitivity showed that other physical factors had no important impact on the wave characteristics.

Choosing the right whitecapping formulation and its related parameters is a critical component of a reliable wave model [48,49]. It is found that whitecapping formulations that use average spectral properties provide the most accurate representation of total energy in the higher frequency part of a combined sea state which is related to local waves [50]. The Komen-type approaches of whitecapping modeling are one of widely used methods and originated from Hasselmann, formulated by Komen et al., and enhanced by Janssen [22]. Equations (3)–(5) are utilized in Mike21 SW to describe the energy dissipation rate caused by whitecapping:

$$S_{ds}(f.\theta) = -C_{ds} \left(\frac{\widehat{\alpha}}{\alpha_{PM}} \right)^m \left\{ (1-\delta)\frac{k}{\overline{k}} + \delta \left(\frac{k}{\overline{k}} \right)^2 \right\} \overline{\sigma} E(f.\theta) \tag{3}$$

$$\alpha_{PM} = \left(3.02 \times 10^{-3} \right)^{1/2} \tag{4}$$

$$\widehat{\alpha} = \overline{k} \sqrt{E_{\text{tot}}} \tag{5}$$

where C_{ds} represents the white capping coefficient with default value of 4.5. Although, it can be considered as a calibration parameter for deep-water waves. It is possible to partially calibrate wave period by modifying parameter δ, which has a default value of 0.5 [22]. In addition, k represents wave number the average of k. Parameter m is assumed to be 1 based on WAMDI group studies [51]. Finally, E_{tot} and σ are the total energy of the wave spectrum and average angular velocity, respectively. Therefore, in this study, for calibration purposes, the parameters C_{ds} and δ (whitecapping dissipation coefficients) for the Arabian Sea were adjusted to 0.5 and 2.5, respectively.

ECMWF ERA5 data were used to generate the wind field of the Kyarr cyclone during its passage. Every three hours, the results were compared to data from the Chabahar meteorology synoptic station. Using data from the Chabahar meteorological synoptic station, the wind field modeled with ECMWF ERA5 data was validated. The generated wind field accurately captured [Root Mean Square Errors (RMSE) is 0.79] the wind speed during cyclone passage from the study region (Figure 6). Figure 6 shows that the numerical results of the wind speed at the peak wind speed using reanalyses data from the ECMWF ERA5 have successfully simulated the wind field, and the result on 10/30/2019 at 9:00 AM is very close to the real values. Wind and pressure fields of tropical cyclones are estimated using analytical formulas.
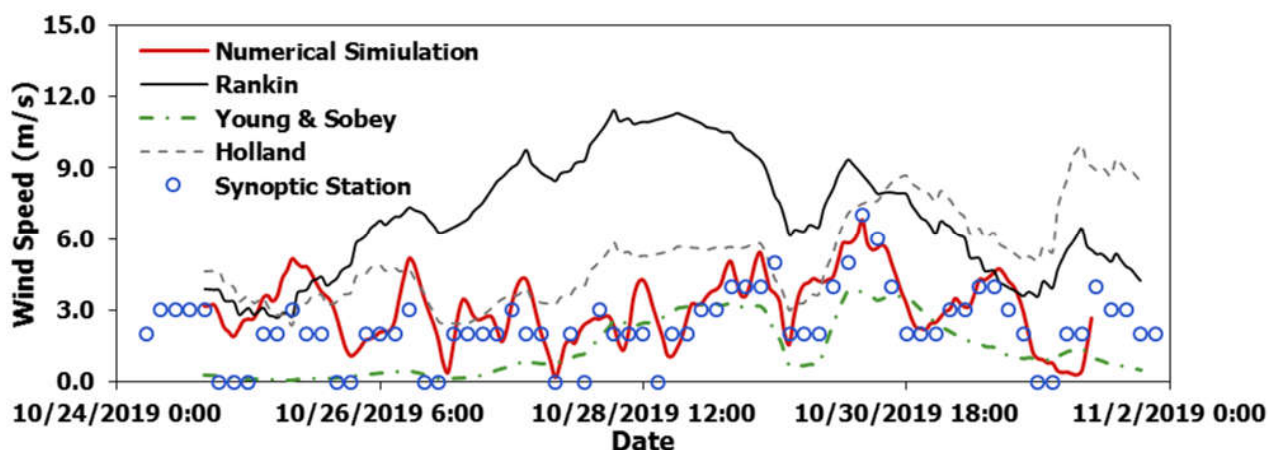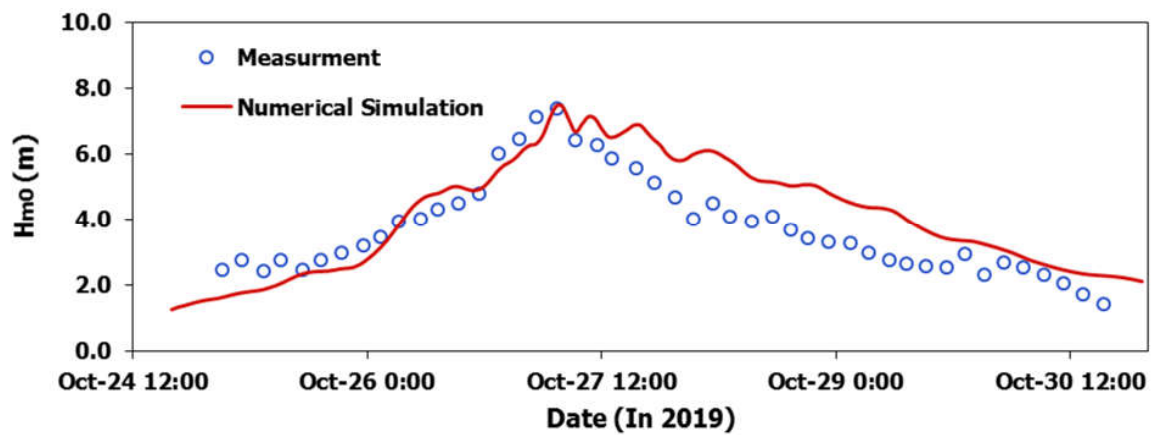

Figure 6. Comparison of the wind speed from simulations and meteorological synoptic data during tropical cyclone Kyarr at the Chabahar station.
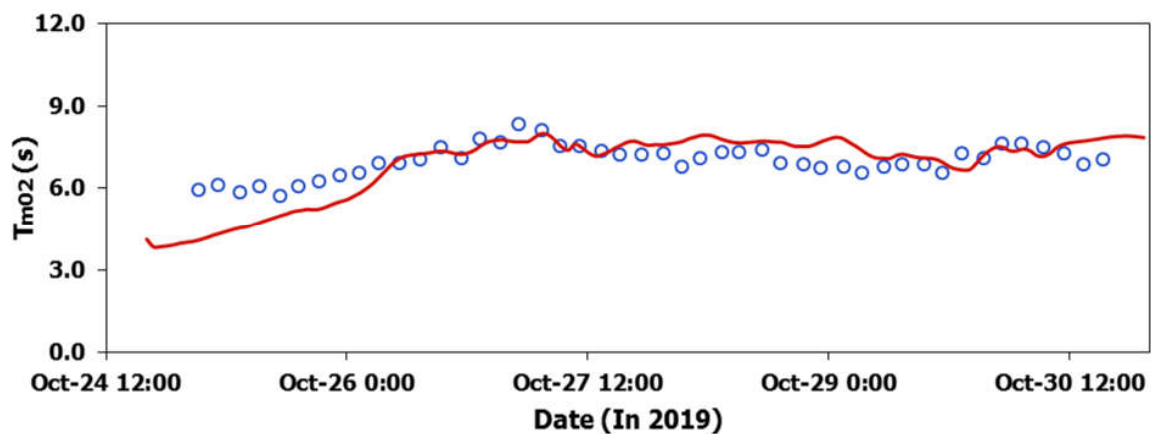
Analytical and parametric models for tropical cyclones surface wind distribution are commonly utilized for risk evaluations [52]. Analytical wind models employ an idealized cyclone, which may lead to erroneous wind field representations far from the cyclone's center [44]. Additionally, the MIKE 21 Cyclone Wind Generation was applied in this study to generate the cyclone's wind field. Wind fields were generated using the Young and Sobey (1981), Holland (1980), and Rankine (1872) vortex models during the passage of the Kyarr cyclone. The model requires cyclone position, center pressure, maximum sustained wind speed, and maximum wind radius (RVmax) as input variables. Using the International Best Track Archive for Climate Stewardship (IBTrACS) global tropical cyclone database, these statistics were compiled. The comparison between analytical wind models and observed peak wind speed for the Kyarr cyclone reveals that while simulations with the ECMWF ERA5 dataset perform well, the Young and Sobey model underestimates the wind speed measured at the Chabahar station. Meanwhile, Rankine and Holland models typically overestimate the wind speed (Figure 6).

In Figure 7, a comparison of the measured and modeled wave parameters demonstrates that the modeled significant wave heights closely match the observed data with highest significant wave height, at 7.5 m. As well, the mean wave periods closely match the observation data. For T_{m02} and H_{m0}, Correlation Coefficients (CC) of 0.64 and 0.095,
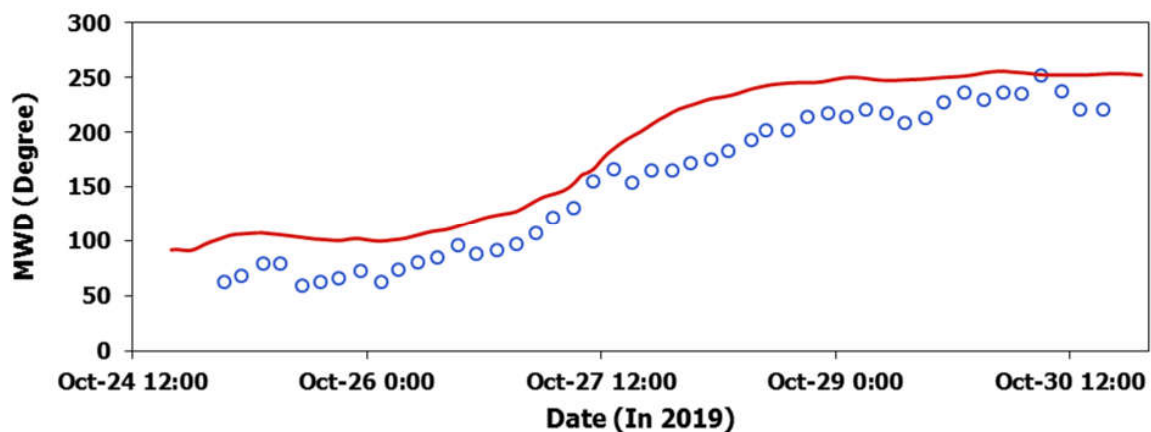
RMSE of 0.65 s and 0.34 m, Biases of +0.39 s and 0.19 m, and Scattering Indexes (SI) of 0.075 and 0.092 were calculated, respectively.

(a)

(b)

(c)

Figure 7. Comparison of the (**a**) wave height and (**b**) wave period (**c**) wave direction from simulation and measurement data during tropical cyclone Kyarr.

Finally, for the model validation, the significant wave heights extracted from the model results were compared with the satellite altimeter data for tropical cyclone Kyarr. The National Oceanic and Atmospheric Administration (NOAA) CoastWatch/OceanWatch Portal was implemented to acquire the satellite altimeter data in this study. As shown in Figure 8, for a thorough evaluation of the wave heights along the cyclone tracks, this

research examined all the data spanning the Arabian Sea for the duration of tropical cyclone Kyarr (obtained from CryoSat-2, SARAL and Jason-3 satellite altimeter data). The scatter plot of the satellite altimeter data against the model results (Figure 9) demonstrates a very close correspondence. The comparison result is acceptable, with a CC of 0.88, a RMSE of 0.83 m, a Bias of 0.36 m, and a Scattering Index of 0.20. The validation demonstrates a high degree of agreement, given the research area's size.

Figure 8. Location of satellite altimeter measurements of wave height during tropical Cyclone Kyarr.
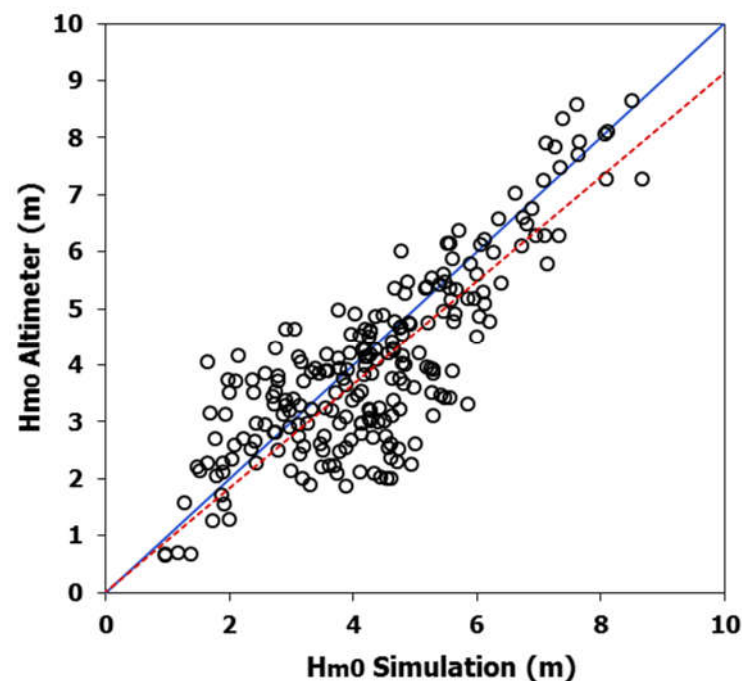

Figure 9. Satellite altimeter wave data against Mike 21 SW model results during tropical cyclone Kyarr (the blue line is x = y and redline is trendline).

3. Results and Discussion

The tropical cyclone Kyarr was numerically simulated utilizing the ECMWF ERA5 dataset as wave and wind inputs. The run was conducted using a 3rd generation wave model of MIKE 21 SW. The outputs of this simulation was examined at various locations across the Arabian Sea.

Statistical analysis of the model results was conducted to evaluate the maximum significant wave conditions throughout the entire model domain during the tropical cyclone Kyarr. On 28 October 2019, at 23:00:00, a significant wave height of approximately 10.7 m (with corresponding peak wave period of 12.5 s) was observed at 63.049 E, 19.959 N. (Figure 10). As shown in Figure 10, for this time step isoline, the maximum significant wave height is almost parallel to the Iranian and Pakistani coasts. Additionally, Figure 10 illustrates 13 points along the cyclone's track where the model results were extracted.
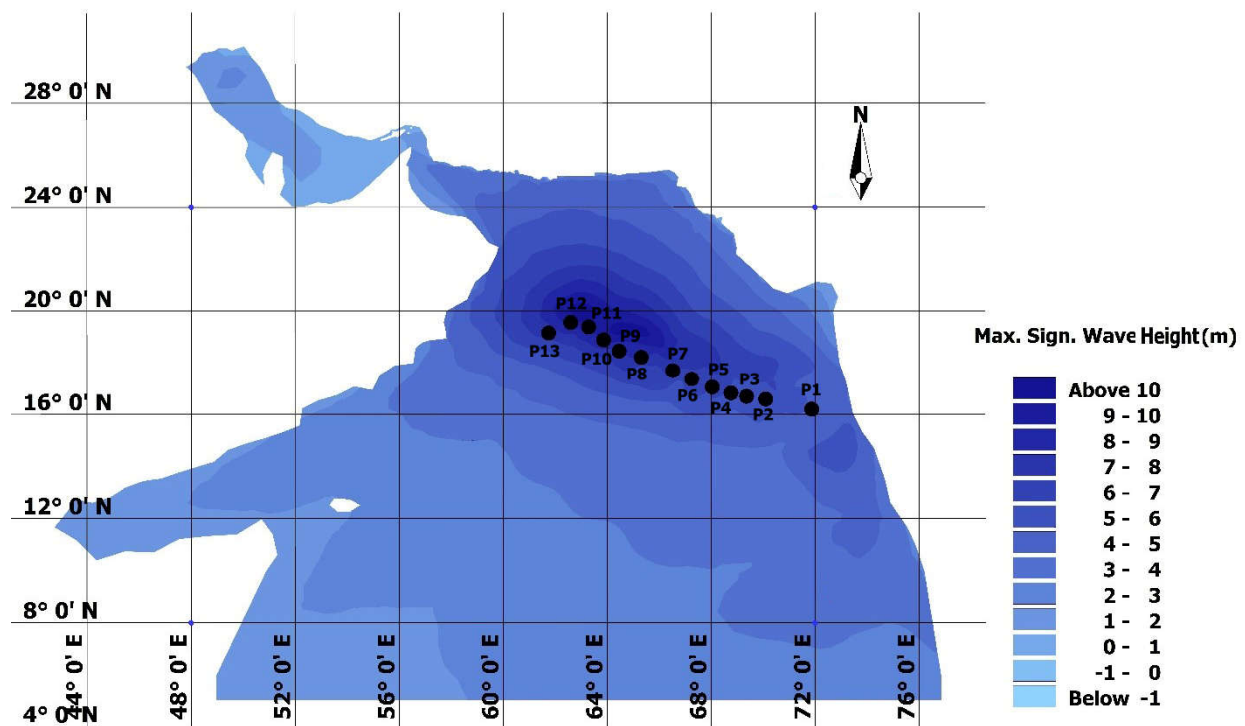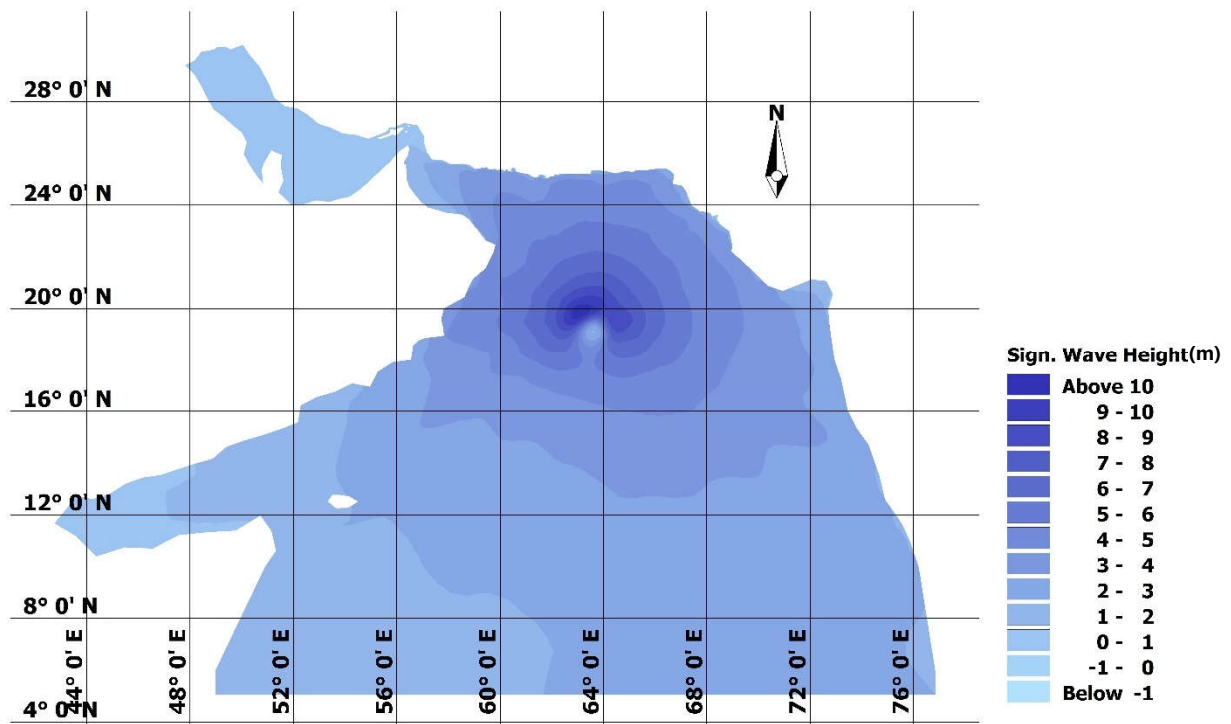

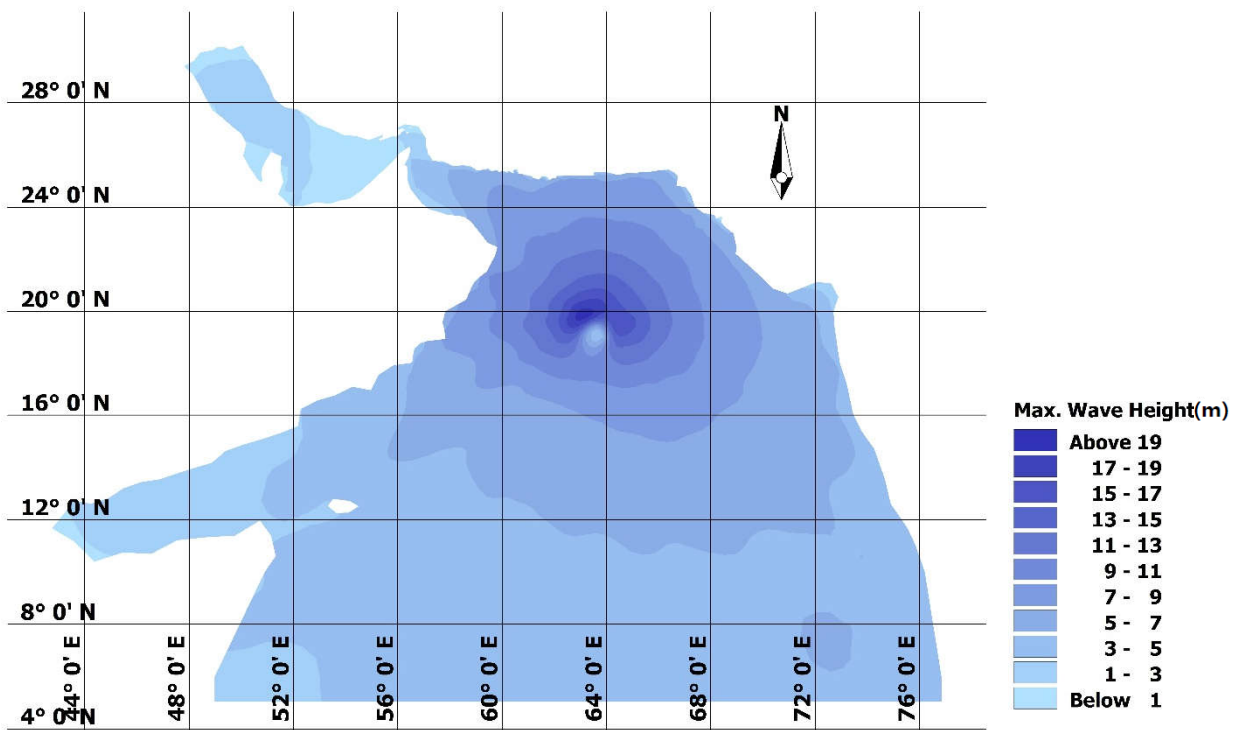**Figure 10.** Optional points along tropical cyclone Kyarr.

The patterns of the significant wave height, the maximum wave height, the wind speed and the peak weave period for the above-mentioned time step are illustrated in Figure 11. Figure 11a shows that maximum significant wave height during simulation, which occurred near the central area of the Arabian Sea. As shown in the Figure 11, the maximum wave height and the peak wave period for this time step were approximately 19.8 m and 16.7 s, respectively. Furthermore, the results showed that significant wave heights of more than 9 m could only last for approximately 28 h.

To compare the significant wave heights at different locations along the cyclone track, the maximum significant wave heights were displayed in Figure 12. As shown in Figure 12, around the central area of the Arabian Sea, the significant wave height became significantly higher than in other areas.

Maximum wave heights were derived from the modeling results for the study region throughout tropical cyclone Kyarr (Figure 13). During simulation, the maximum wave height was 19.8 m at 63.188° E, 19.847° N.
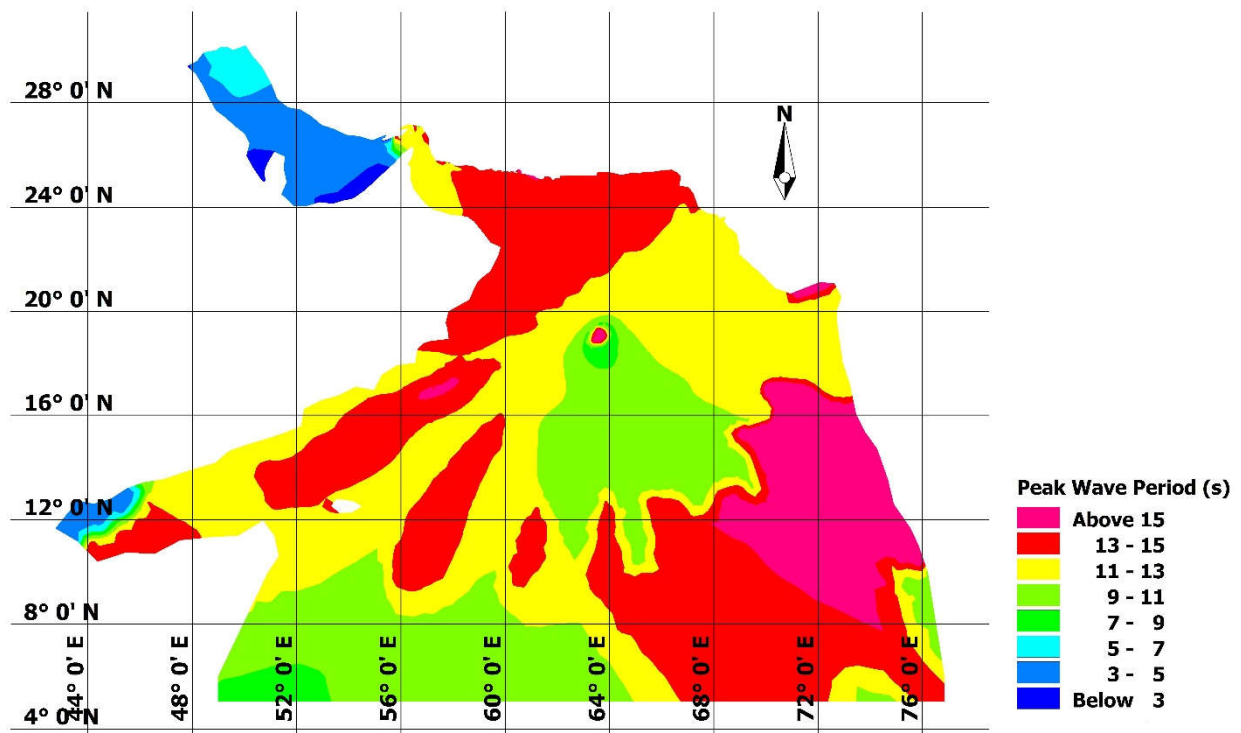
(**a**)

(**b**)

Figure 11. *Cont.*

(**c**)

Figure 11. Wave parameters pattern in the computational domain (**a**) significant wave height, (**b**) maximum wave height, and (**c**) peak wave period.
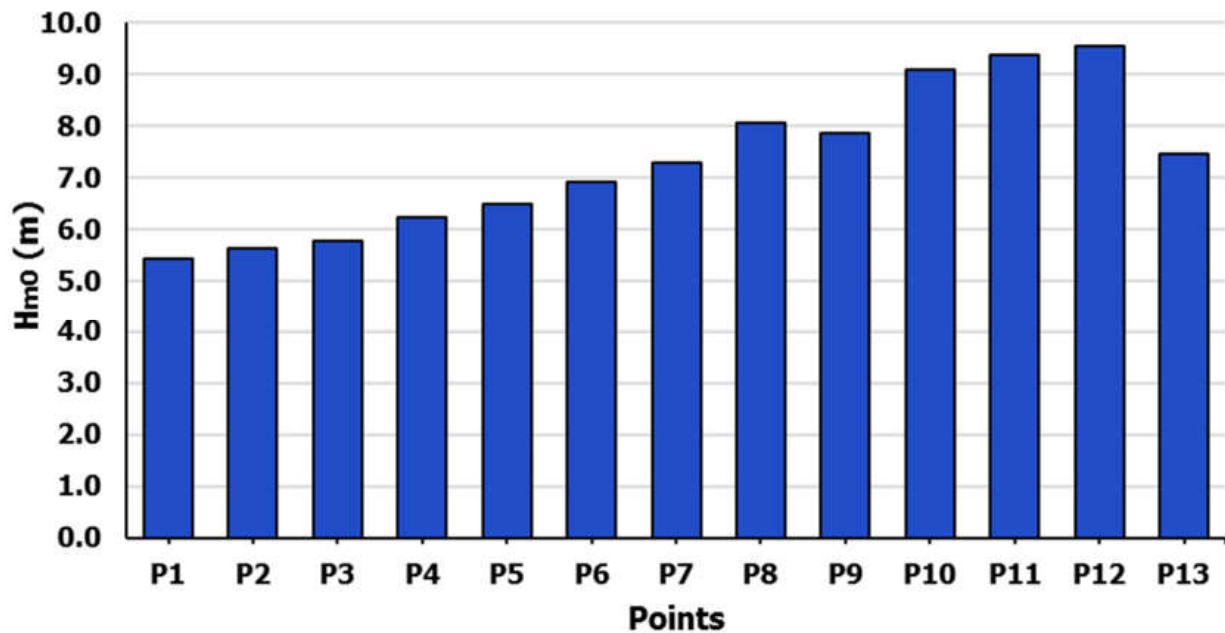

Figure 12. Wave height at optional points along tropical cyclone Kyarr track.
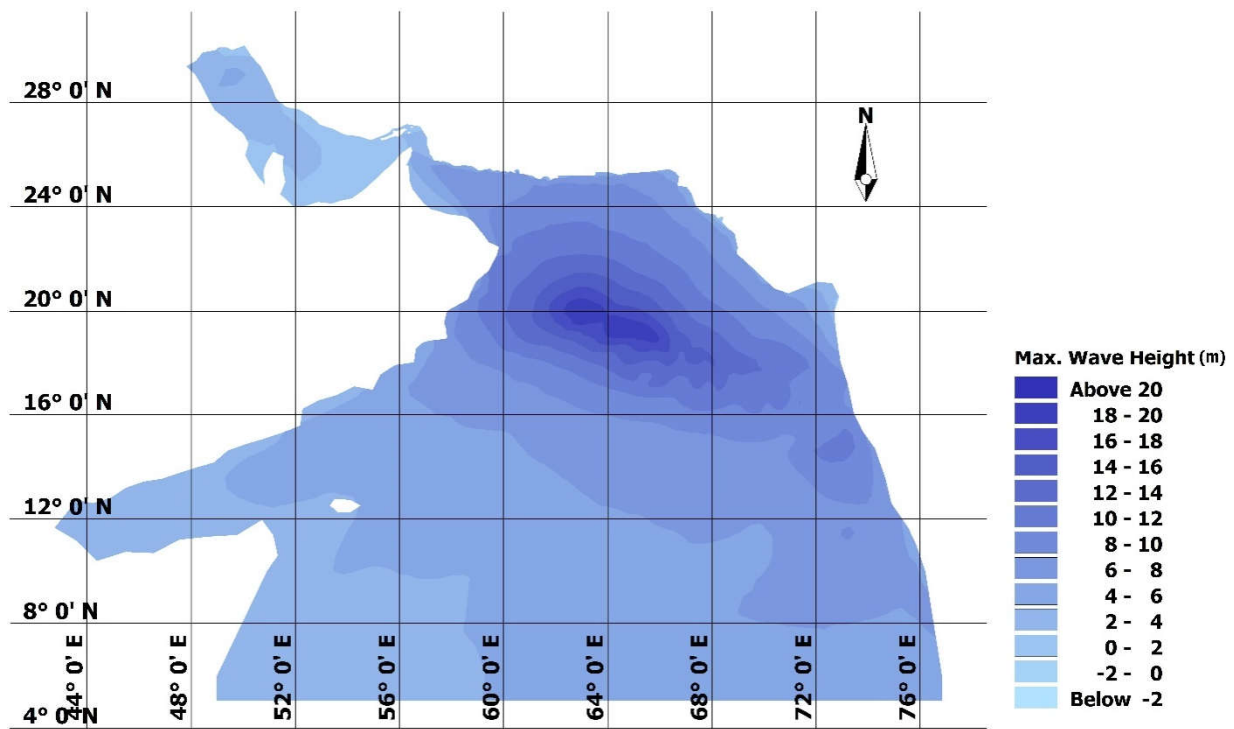
Figure 13. Maximum wave height in the study area during tropical cyclone Kyarr.

Figure 14 indicates that significant wave heights were reached along the Iranian and Pakistani coasts (north Arabian Sea) to a range of 1.4–2.8 m as tropical cyclone Kyarr moved north. Kyarr became a Super Cyclonic Storm, resulting in significant wave heights in the range of 1.5–3.5 m along Ormara, Gaddani, Konarak, Pasni, Gwatr, and Chabahar (See Figure 14). Therefore, the significant wave height is lower along the northwest and northeast coasts of the Arabian Sea than along the northern coasts.
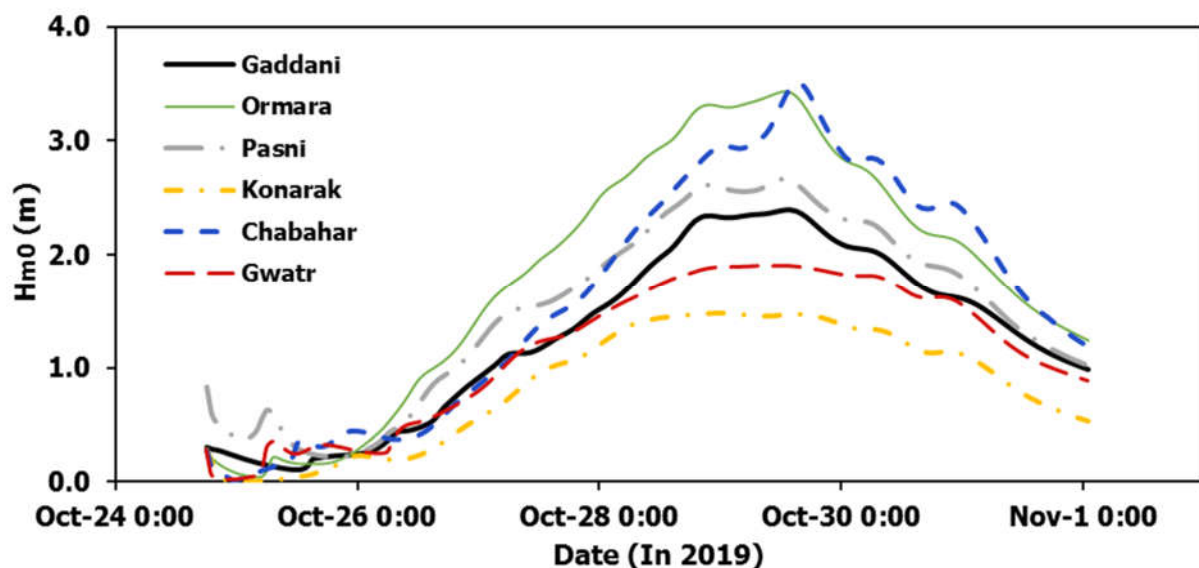

Figure 14. Significant wave heights along the Iranian and Pakistani coastlines during tropical cyclone Kyarr.

4. Conclusions

Based on an 8-day period of numerical simulations of tropical cyclone Kyarr (2019), this study investigates the wave characteristics in the Arabian Sea and the Gulf of Oman.

Tropical cyclone Kyarr's (2019) wave generation is validated using offshore wave observations and satellite altimeter data. If no field data is available, altimeter data was used to validate model results. Wind data from the ECMWF ERA5 model were also employed to force wind field throughout the tropical cyclone Kyarr's passage. Conclusions are listed below:

(1) Cyclone model simulations indicated that the maximum significant wave height occurred throughout tropical cyclone Kyarr was 10.7 m. The maximum significant wave height occurred at 63.049° E, 19.959° N, approximately 400 km off the coast of Oman. Significant wave heights along the Iranian coast reached up to 3.51 m at Chabahar Port (60.619° E, 25.264° N) and up to 3.45 m in Pakistan's coasts (Ormara, 64.700° E, 25.215° N) during Kyarr's upgrade to Super Cyclonic Storm;

(2) Using the ECMWF ERA5 input data, the model captured the wind field generated by tropical cyclone Kyarr in the studied region with high accuracy. This study showed that the MIKE 21 SW model could successfully hindcast the tropical cyclone waves using ERA5 wind field;

(3) The model's outputs may be employed as inputs for research on coastal planning, management, and risk assessment. Additionally, the validated model may be utilized for forecast purpose. As a consequence of the sea-level rise, cyclonic wave conditions nearshore may increase, potentially resulting in greater coastal erosion and floods. Forecasting cyclone-generated waves allows for the prediction of the possible effects on the shore.

References

1. Tasnim, K.M.; Shibayama, T.; Esteban, M.; Takagi, H.; Ohira, K.; Nakamura, R. Field Observation and Numerical Simulation of Past and Future Storm Surges in the Bay of Bengal: Case Study of Cyclone Nargis. *Nat. Hazards* **2015**, *75*, 1619–1647. [CrossRef]
2. Yavari, F.; Salehi Neyshabouri, S.A.; Yazdi, J.; Molajou, A.; Brysiewicz, A. A Novel Framework for Urban Flood damage Assessment. *Water Resour. Manag* **2022**, *36*, 1991–2011. [CrossRef]
3. Azizi, H.; Nejatian, N. Evaluation of the climate change impact on the intensity and return period for drought indices of SPI and SPEI (study area: Varamin plain). *Water Supply* **2022**, *22*, 4373–4386. [CrossRef]
4. Ramsay, H.A.; Singh, M.S.; Chavas, D.R. Response of Tropical Cyclone Formation and Intensification Rates to Climate Warming in Idealized Simulations. *J. Adv. Modeling Earth Syst.* **2020**, *12*. [CrossRef]
5. Booth, J.F.; Narinesingh, V.; Towey, K.L.; Jeyaratnam, J. Storm Surge, Blocking, and Cyclones: A Compound Hazards Analysis for the Northeast United States. *J. Appl. Meteorol. Climatol.* **2021**, *60*, 1531–1544. [CrossRef]
6. Costanza, R.; Anderson, S.J.; Sutton, P.; Mulder, K.; Mulder, O.; Kubiszewski, I.; Wang, X.; Liu, X.; Pérez-Maqueo, O.; Luisa Martinez, M.; et al. The Global Value of Coastal Wetlands for Storm Protection. *Glob. Environ. Chang.* **2021**, *70*, 102328. [CrossRef]
7. Banan-Dallalian, M.; Shokatian-Beiragh, M.; Golshani, A.; Mojtahedi, A.; Lotfollahi-Yaghin, M.A. Study of the Effect of Gonu Tropical Cyclone on the Oman Coastlines Inland Flooding (Case Study: The Coastline of Sur). In Proceedings of the 2nd International Conference on Oceanography for West Asia (RCOWA 2020), Tehran, Iran, 16–17 September 2020.
8. Mojtahedi, A.; Beiragh, M.S.; Farajpour, I.; Mohammadian, M. Investigation on Hydrodynamic Performance of an Environmentally Friendly Pile Breakwater. *Ocean Eng.* **2020**, *217*, 107942. [CrossRef]
9. Hereher, M.; Al-Awadhi, T.; Al-Hatrushi, S.; Charabi, Y.; Mansour, S.; Al-Nasiri, N.; Sherief, Y.; El-Kenawy, A. Assessment of the Coastal Vulnerability to Sea Level Rise: Sultanate of Oman. *Environ. Earth Sci.* **2020**, *79*, 369. [CrossRef]

10. Ibrahim, O.R.; Al Maghawry, S. Review on Cyclone Shaheen in the Sultanate of Oman. *Arab. J. Geosci.* **2022**, *15*, 833. [CrossRef]
11. Fritz, H.M.; Blount, C.D.; Albusaidi, F.B.; Al-Harthy, A.H.M. Cyclone Gonu Storm Surge in Oman. *Estuar. Coast. Shelf Sci.* **2010**, *86*, 102–106. [CrossRef]
12. Krishna, K.M.; Rao, S.R. Study of the Intensity of Super Cyclonic Storm GONU Using Satellite Observations. *Int. J. Appl. Earth Obs. Geoinf.* **2009**, *11*, 108–113. [CrossRef]
13. Wang, Z.; DiMarco, S.F.; Stössel, M.M.; Zhang, X.; Howard, M.K.; du Vall, K. Oscillation Responses to Tropical Cyclone Gonu in Northern Arabian Sea from a Moored Observing System. *Deep-Sea Res. Part I Oceanogr. Res. Pap.* **2012**, *64*, 129–145. [CrossRef]
14. Soltanpour, M.; Ranji, Z.; Shibayama, T.; Ghader, S. Tropical Cyclones in the Arabian Sea: Overview and Simulation of Winds and Storm-Induced Waves. *Nat. Hazards* **2021**, *108*, 711–732. [CrossRef]
15. Nair, M.A.; Amrutha, M.M.; Kumar, V.S. Spectral Wave Characteristics in the Coastal Waters of the Central West Coast of India during Tropical Cyclone Kyarr. *Ocean. Dyn.* **2022**, *72*, 151–168. [CrossRef]
16. Dibajnia, M.; Soltanpour, M.; Nairn, R.; Allahyar, M. Cyclone Gonu: The Most Intense Tropical Cyclone on Record in the Arabian Sea. In *Indian Ocean Tropical Cyclones and Climate Change*; Springer: Dordrecht, Netherlands, 2010; pp. 149–157, ISBN 9789048131082.
17. Sarker, M.A. Cyclone Hazards in the Arabian Sea–A Numerical Modelling Case Study of Cyclone Nilofar. *Water Environ. J.* **2017**, *31*, 284–295. [CrossRef]
18. Bakhtiari, A.; Allahyar, M.R.; Jedari Attari, M.; Haghshenas, S.A.; Bagheri, M. Modeling of Last Recent Tropical Storms in the Arabian Sea. *J. Coast. Mar. Eng.* **2018**, *1*, 58–66.
19. Golshani, A.; Taebi, S. Numerical Modeling and Warning Procedure for Gonu Super Cyclone along Iranian Coastlines. In Proceedings of the Solutions to Coastal Disasters Congress 2008, Oahu, HI, USA, 13–16 April 2008; Volume 312, pp. 268–275.
20. Jayakrishnan, P.R.; Babu, C.A. Study of the Oceanic Heat Budget Components over the Arabian Sea during the Formation and Evolution of Super Cyclone, Gonu. *Atmos. Clim. Sci.* **2013**, *3*, 282–290. [CrossRef]
21. Ghader, S.; Yazgi, D.; Haghshenas, S.A.; Arab, A.R.; Attari, M.J.; Bakhtiari, A.; Zinsazboroujerdi, H. Hindcasting Tropical Storm Events in the Oman Sea. *J. Coast. Res.* **2016**, *1*, 1087–1091. [CrossRef]
22. Allahdadi, M.N.; Chaichitehrani, N.; Allahyar, M.; McGee, L. Wave Spectral Patterns during a Historical Cyclone: A Numerical Model for Cyclone Gonu in the Northern Oman Sea. *Open J. Fluid Dyn.* **2017**, *7*, 131–151. [CrossRef]
23. Allahdadi, M.N.; Chaichitehrani, N.; Jose, F.; Nasrollahi, A.; Afshar, A.; Allahyar, M. Cyclone-Generated Storm Surge in the Northern Gulf of Oman: A Field Data Analysis during Cyclone Gonu. *Am. J. Fluid Dyn.* **2018**, *8*, 10–18.
24. Sarker, M.A. Numerical Modelling of Waves and Surge from Cyclone Mekunu (May 2018) in the Arabian Sea. *J. Atmos. Sci. Res.* **2020**, *2*, 12–20. [CrossRef]
25. Banan-Dallalian, M.; Shokatian-Beiragh, M.; Golshani, A.; Mojtahedi, A.; Lotfollahi-Yaghin, M.A.; Akib, S. Study of the Effect of an Environmentally Friendly Flood Risk Reduction Approach on the Oman Coastlines during the Gonu Tropical Cyclone (Case Study: The Coastline of Sur). *Eng* **2021**, *2*, 141–155. [CrossRef]
26. Vieira, F.; Cavalcante, G.; Campos, E. Simulation of Cyclonic Wave Conditions in the Gulf of Oman. *Nat. Hazards* **2021**, *105*, 2203–2217. [CrossRef]
27. Li, J.; Pan, S.; Chen, Y.; Pan, Y. Assessment of Tropical Cyclones in Ecmwf Reanalysis Data over Northwest Pacific Ocean. In Proceedings of the 27th International Ocean and Polar Engineering Conference, San Francisco, CA, USA, 25–30 June 2017.
28. Yu, Y.C.; Chen, H.; Shih, H.J.; Chang, C.H.; Hsiao, S.C.; Chen, W.B.; Chen, Y.M.; Su, W.R.; Lin, L.Y. Assessing the Potential Highest Storm Tide Hazard in Taiwan Based on 40-Year Historical Typhoon Surge Hindcasting. *Atmosphere* **2019**, *10*, 346. [CrossRef]
29. Li, J.; Pan, S.; Chen, Y.; Fan, Y.M.; Pan, Y. Numerical Estimation of Extreme Waves and Surges over the Northwest Pacific Ocean. *Ocean Eng.* **2018**, *153*, 225–241. [CrossRef]
30. Hodges, K.; Cobb, A.; Vidale, P.L. How Well Are Tropical Cyclones Represented in Reanalysis Datasets? *J. Clim.* **2017**, *30*, 5243–5264. [CrossRef]
31. Pan, Y.; Chen, Y.-p.; Li, J.-x.; Ding, X.-l. Improvement of Wind Field Hindcasts for Tropical Cyclones. *Water Sci. Eng.* **2016**, *9*, 58–66. [CrossRef]
32. Malakar, P.; Kesarkar, A.P.; Bhate, J.N.; Singh, V.; Deshamukhya, A. Comparison of Reanalysis Data Sets to Comprehend the Evolution of Tropical Cyclones Over North Indian Ocean. *Earth Space Sci.* **2020**, *7*, e2019EA000978. [CrossRef]
33. Chaichitehrani, N.; Allahdadi, M.N. Overview of Wind Climatology for the Gulf of Oman and the Northern Arabian Sea. *Am. J. Fluid Dyn.* **2018**, *8*, 1–9. [CrossRef]
34. Siahsarani, A.; Karami Khaniki, A.; Aliakbari Bidokhti, A.A.; Azadi, M. Sensitivity Analysis of the Numerical Aspect of the SWAN for the Tropical Cyclone Wave Simulations in the Gulf of Oman. *Arab. J. Geosci.* **2020**, *13*, 692. [CrossRef]
35. Sahoo, B.; Bhaskaran, P.K. A Comprehensive Data Set for Tropical Cyclone Storm Surge-Induced Inundation for the East Coast of India. *Int. J. Climatol.* **2018**, *38*, 403–419. [CrossRef]
36. Komen, G.J.; Cavaleri, L.; Donelan, M.; Hasselmann, K.; Hasselmann, S.; Janssen, P.A.E.M. *Dynamics and Modelling of Ocean Waves*; Cambridge University Press: Cambridge, UK, 1994.
37. Young, I.R. Seasonal Variability of the Global Ocean Wind and Wave Climate. *Int. J. Climatol.* **1999**, *19*, 931–950. [CrossRef]
38. DHI Company. *Dhi MIKE 21-Spectral Wave Module-Scientific Document*; DHI Water & Environment: Hørsholm, Denmark, 2007; Volume 42.
39. Weisberg, R.H.; Zheng, L. Hurricane Storm Surge Simulations for Tampa Bay. *Estuaries Coasts* **2006**, *29*, 899–913. [CrossRef]

40. Rego, J.L.; Li, C. On the Importance of the Forward Speed of Hurricanes in Storm Surge Forecasting: A Numerical Study. *Geophys. Res. Lett.* **2009**, *36*. [CrossRef]

41. Kennedy, A.B.; Westerink, J.J.; Smith, J.M.; Hope, M.E.; Hartman, M.; Taflanidis, A.A.; Tanaka, S.; Westerink, H.; Cheung, K.F.; Smith, T.; et al. Tropical Cyclone Inundation Potential on the Hawaiian Islands of Oahu and Kauai. *Ocean Model.* **2012**, *52–53*, 54–68. [CrossRef]

42. Sochala, P.; Chen, C.; Dawson, C.; Iskandarani, M. A Polynomial Chaos Framework for Probabilistic Predictions of Storm Surge Events. *Comput. Geosci.* **2020**, *24*, 109–128. [CrossRef]

43. Chao, W.T.; Young, C.C.; Hsu, T.W.; Liu, W.C.; Liu, C.Y. Long-Lead-Time Prediction of Storm Surge Using Artificial Neural Networks and Effective Typhoon Parameters: Revisit and Deeper Insight. *Water* **2020**, *12*, 2394. [CrossRef]

44. Phadke, A.C.; Martino, C.D.; Cheung, K.F.; Houston, S.H. Modeling of Tropical Cyclone Winds and Waves for Emergency Management. *Ocean Eng.* **2003**, *30*, 553–578. [CrossRef]

45. Kazeminezhad, M.H.; Etemad-Shahidi, A.; Mousavi, S.J. Evaluation of Neuro Fuzzy and Numerical Wave Prediction Models in Lake Ontario. *J. Coast. Res.* **2007**, *SI 50*, 317–321.

46. van der Westhuysen, A.J.; Zijlema, M.; Battjes, J.A. Nonlinear Saturation-Based Whitecapping Dissipation in SWAN for Deep and Shallow Water. *Coast. Eng.* **2007**, *54*, 151–170. [CrossRef]

47. Ribal, A.; Young, I.R. 33 Years of Globally Calibrated Wave Height and Wind Speed Data Based on Altimeter Observations. *Sci. Data* **2019**, *6*, 77. [CrossRef]

48. Allahdadi, M.N.; He, R.; Ahn, S.; Chartrand, C.; Neary, V.S. Development and Calibration of a High-Resolution Model for the Gulf of Mexico, Puerto Rico, and the U.S. Virgin Islands: Implication for Wave Energy Resource Characterization. *Ocean Eng.* **2021**, *235*, 109304. [CrossRef]

49. Allahdadi, M.N.; Gunawan, B.; Lai, J.; He, R.; Neary, V.S. Development and Validation of a Regional-Scale High-Resolution Unstructured Model for Wave Energy Resource Characterization along the US East Coast. *Renew. Energy* **2019**, *136*, 500–511. [CrossRef]

50. Nabi Allahdadi, M.; He, R.; Neary, V.S. Predicting Ocean Waves along the US East Coast during Energetic Winter Storms: Sensitivity to Whitecapping Parameterizations. *Ocean Sci.* **2019**, *15*, 691–715. [CrossRef]

51. WAMDI Group The WAM Model—A Third Generation Ocean Wave Pre-Diction Model. *J. Phys. Oceanogr.* **1988**, *18*, 1775–1810. [CrossRef]

52. Wang, S.; Lin, N.; Gori, A. Investigation of Tropical Cyclone Wind Models With Application to Storm Tide Simulations. *J. Geophys. Res. Atmos.* **2022**, *127*, e2021JD036359. [CrossRef]